Coherent stochastic resonance in the case of two absorbing boundaries

Asish K. Dhara and Tapan Mukhopadhyay
Variable Energy Cyclotron Centre, 1/AF Bidhan Nagar, Calcutta 700064, India
(Received 15 January 1999)

The coherent stochastic resonance is observed and studied with a multistep periodic signal in a continuous medium having two absorbing boundaries. The general features of this process are exhibited. The universal features at the resonance point are demonstrated. The kinetic behaviors around the resonance point are also presented. [S1063-651X(99)10409-4]

PACS number(s): 05.40.−a

I. INTRODUCTION

There has been a great deal of interest in the understanding of the mechanism of interplay between random noise and a deterministic periodic signal after the pioneering achievement of the separation of large DNA molecules in a gel medium by the application of a uniform and time-dependent periodic electric field [1,2]. It has been found that with this technique, large molecules in the size range 2–400 kb exhibit size-dependent mobilities. Similar ideas have also arisen in other types of chromatographic processes [3].

The first-passage time is a useful tool with which to investigate the diffusive transport property in a medium. The theory of first-passage time has been worked out in great detail for both an infinite medium and explicitly time-independent diffusive processes [4–6]. However, for explicitly time-dependent processes and in a finite medium, analytic closed-form expressions are not available. In this respect also this problem has attracted much attention in the scientific community.

The first analysis of this phenomenon has been done for a random walk on a lattice numerically, and for a diffusive process in a continuous medium with a periodic signal of small amplitude perturbatively [7]. Their results indicate that the oscillating field can create a form of coherent motion capable of reducing the first-passage time by a significant amount. This fact clearly implies that the mobility of a particle in a diffusive medium can be increased by the application of a proper oscillating field. This phenomenon is known in the literature as coherent stochastic resonance (CSR).

In order to investigate the reason for this cooperative behavior of random noise and a deterministic periodic signal, this problem has been formulated in much simpler terms by approximating the sinusoidal periodic signal by the telegraph signal [8] and it was concluded incorrectly that the system exhibits CSR. Subsequently, it has been shown [9] that the telegraph signal cannot produce CSR. It was then argued [9] that the low-frequency behavior could cause such cooperative behavior.

In this paper we approximate the sinusoidal signal by a multistep periodic signal (explained below) and obtain an expression for the mean first-passage time (MFPT). After giving the derivation of MFPT in Sec. II, the results of the calculations are discussed in Sec. III. First, we present the general characteristics of CSR. The calculation clearly exhibits how resonance appears in our multistep approximation and fails to show in the single-step telegraph approximation of the periodic signal explaining the conjecture of Porra [9]. The general characteristics of the moments in our calculation are also in agreement with the numerical simulation of the random-walk model on a lattice [7]. The characteristic features of the first-passage time density function (FPTDF) for this phenomenon are also presented in this subsection. In the next subsection we focus on the resonance point and demonstrate some universal features associated with it. The subsequent subsection deals with the characteristic changes of the physical variables as we cross, in particular, around the resonance point. This leads to a better understanding of this cooperative behavior. Finally, a few concluding remarks have been added in Sec. IV.

II. DERIVATION OF THE MEAN FIRST-PASSAGE TIME

We consider diffusion in one dimension perturbed by a periodic force. The motion of the particle is given by the Langevin equation

$$\dot{X} = A \sin \Omega t + \xi(t), \tag{1}$$

where X refers to the stochastic variable, A and Ω are the amplitude and frequency of the sinusoidal signal, and $\xi(t)$ is a zero mean Gaussian white noise of strength D with the autocorrelation function given by

$$\langle \xi(t)\xi(t') \rangle = 2D\delta(t-t'). \tag{2}$$

The motion is confined between two absorbing boundaries at $x=0$ and $x=L$. The Fokker-Planck equation corresponding to Eq. (1) is

$$\frac{\partial p(x,t)}{\partial t} = -A \sin \Omega t \frac{\partial p(x,t)}{\partial x} + D \frac{\partial^2 p(x,t)}{\partial x^2}, \tag{3}$$

with absorbing boundary conditions at $x=0$ and $x=L$; i.e., $p(0,t)=p(L,t)=0$. We now introduce the dimensionless variables

$$\xi = (A/D)x, \quad \theta = (A^2/D)t, \quad \omega = \Omega/(A^2/D), \tag{4}$$

to write Eq. (3) in terms of new variables:

$$\frac{\partial p(\xi,\theta)}{\partial \theta} = -\sin \omega\theta \frac{\partial p(\xi,\theta)}{\partial \xi} + \frac{\partial^2 p(\xi,\theta)}{\partial \theta^2}. \tag{5}$$

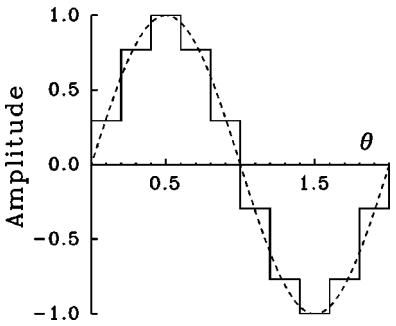

FIG. 1. Sinusoidal signal (dashed curve) and approximated three-step ($p=2$) periodic signal (solid curve) for the full one cycle as a function of θ.

The boundary conditions are rewritten as $p(0,\theta)=p(\Lambda,\theta)=0$, where $\Lambda=(A/D)L$. In the following we calculate all the physical quantities in terms of these new variables and, if required, one may translate all the interpretations in terms of the usual variables by the transformation equations (4).

We next approximate the sinusoidal signal by the multistep periodic signal. The construction is as follows. We divide the half-cycle of the signal by $(2p+1)$ intervals so that each interval in the horizontal θ axis is of size $[\Delta\theta/(2p+1)]$ with $\omega\Delta\theta=\pi$. We define $(2p+1)$ numbers s_k along the vertical ξ axis as

$$s_k=\frac{(\sin(k\pi/2p+1)+\sin[(k-1)\pi/2p+1])}{2};$$

$$k=1,2,\ldots,p, \tag{6a}$$

$$s_{p+1}=1, \tag{6b}$$

$$s_{p+1+r}=s_{p+1-r};r=1,2,\ldots,p. \tag{6c}$$

Each number s_k is associated with the interval $(k-1)\Delta\theta/2p+1<\theta\leqslant k\Delta\theta/2p+1$ with $k=1,2,\ldots,(2p+1)$. Equation (6) clearly shows that

$$0<s_1<s_2<\cdots<s_p<s_{p+1}=1>s_{p+2}>s_{p+2}>\cdots>s_{2p+1}>0. \tag{7}$$

Equation (7) states that in order to reach the maximum value $(=1)$ of the signal from the zero level, we have to have $(p+1)$ step up and from the maximum to the zero level we have $(p+1)$ step down. This is for the positive half-cycle. For the negative half-cycle, similar constructions have been done with the replacement $s_k\rightarrow -s_k$, $\forall$ k and each number $-s_k$ is associated with the interval $\Delta\theta[1+(k-1/2p+1)]<\theta\leqslant\Delta\theta[1+(k/2p+1)]$ with $k=1,2,\ldots,(2p+1)$. This approximation for the full one cycle of the sinusoidal signal (as shown in Fig. 1) is then repeated for the next successive cycles. The construction clearly shows that we get back the usual telegraph signal with $p=0$.

One may note, however, that the ω which we have defined for this approximated signal is not the same as that of the sinusoidal signal, because the Fourier transform of the sinusoidal signal would give only one frequency while this approximated signal in the Fourier space corresponds to many sinusoidal frequencies, especially because of its sharp discontinuities. Yet we encourage this approximation because in each interval the equation becomes time-independent.

In future development, we associate the index n with the positive half-cycle and the index m with the negative. Index i will refer to the cycle number. Since the Fokker-Planck equation [Eq. (5)] in each interval will be that for a constant bias, we can express the conditional probability density function $p(\xi,\theta|\xi',\theta')$ in terms of the complete orthonormal set of eigenfunctions $u_n(\xi)$ satisfying the boundary conditions $u_n(0)=u_n(\Lambda)=0$,

$$p(\xi,\theta|\xi',\theta')=\sum_n u_n^+(\xi)u_n^-(\xi')\exp[-\lambda_n(\theta-\theta')], \tag{8}$$

where

$$u_n^{\pm}(\xi)=(2/\Lambda)^{1/2}\exp(\pm s\xi/2)\sin\frac{n\pi\xi}{\Lambda}, \tag{9a}$$

$$\lambda_n=\frac{n^2\pi^2}{\Lambda^2}+\frac{s^2}{4} \tag{9b}$$

with s as the corresponding value of s_k in the appropriate interval where the conditional probability is being decomposed. The conditional probability density function in any interval, say l, can then be calculated from the previous history by convoluting it in each of the previous intervals:

$$p(\xi_l,\theta_l|\xi_1,\theta_1)=\int\cdots\int d\xi_{l-1}d\xi_{l-2}\cdots d\xi_2\times\prod_{j=2}^{l}p(\xi_j,\theta_j|\xi_{j-1},\theta_{j-1}). \tag{10}$$

For the negative half-cycle, the calculation of the probability density function is similar except that we have to replace the index n by m and the probability density function is decomposed as

$$p(\xi,\theta|\xi',\theta')=\sum_m u_m^-(\xi)u_m^+(\xi')\exp[-\lambda_m(\theta-\theta')], \tag{11}$$

where the expressions for $u_m^{\pm}(\xi)$ and λ_m are the same as in Eqs. (9).

The survival probability at time θ when the particle is known to start from $\xi=\xi_0$ at $\theta=0$ is defined as

$$S(\theta|\xi_0)=\int_0^{\Lambda}d\xi\,p(\xi,\theta|\xi_0,0). \tag{12}$$

The first-passage time density function (FPTDF) $g(\theta)$ is defined as

$$g(\theta|\xi_0)=-\frac{dS(\theta|\xi_0)}{d\theta}. \tag{13}$$

Physically, $g(\theta)d\theta$ gives the probability that the particle arrives at any one of the boundaries in the time interval θ and $\theta+d\theta$. From this density function one can calculate various moments:

$$\langle \theta^j \rangle = \int_0^\infty d\theta\, \theta^j g(\theta). \tag{14}$$

From Eq. (14), one can easily calculate the mean first-passage time (MFPT) $\langle \theta \rangle$ and the variance $\sigma^2 = \langle \theta^2 \rangle - \langle \theta \rangle^2$ of the density function $g(\theta)$.

It is then quite straightforward to calculate the survival probability at any interval of any cycle. We will write down the final formulas:

$$S_+(\theta|\xi_0) = C^+_{n_{(2p+1)(i-1)+1}} \exp\{-\lambda_{n_{(2p+1)(i-1)+1}} \times [\theta - 2(i-1)\Delta\theta]\} F_{i-1}(u^-_{n_{(2p+1)(i-1)+1}}),$$

$$2(i-1)\Delta\theta < \theta \leqslant \left(2(i-1)+\frac{1}{2p+1}\right)\Delta\theta, \tag{15a}$$

$$S_+(\theta|\xi_0) = C^+_{n_{(2p+1)(i-1)+(k+1)}} \exp\{-\lambda_{n_{(2p+1)(i-1)+(k+1)}} \times [\theta - 2(i-1)\Delta\theta]\} \times \prod_{j=1}^{k} \{\langle u^-_{n_{(2p+1)(i-1)+(j+1)}} | u^+_{n_{(2p+1)(i-1)+j}} \rangle\} \times \exp\left[\frac{\Delta\theta}{2p+1}\left(k\lambda_{n_{(2p+1)(i-1)+(k+1)}} - \sum_{j=0}^{k-1} \lambda_{n_{(2p+1)(i-1)+(j+1)}}\right)\right] F_{i-1}(u^-_{n_{(2p+1)(i-1)+1}}),$$

$$\left(2(i-1)+\frac{k}{2p+1}\right)\Delta\theta < \theta \leqslant \left(2(i-1)+\frac{(k+1)}{2p+1}\right)\Delta\theta, \quad k = 1,2,\ldots,(2p-1), \tag{15b}$$

$$S_+(\theta|\xi_0) = C^+_{n_{(2p+1)i}} \exp\{-\lambda_{n_{(2p+1)i}}[\theta - (2i-1)\Delta\theta]\} \times A^+(u^-_{n_{(2p+1)i}}, u^+_{n_{(2p+1)(i-1)+1}}) \times F_{i-1}(u^-_{n_{(2p+1)(i-1)+1}}),$$

$$\left(2(i-1)+\frac{2p}{2p+1}\right)\Delta\theta < \theta \leqslant (2i-1)\Delta\theta, \tag{15c}$$

$$S_-(\theta|\xi_0) = C^-_{m_{(2p+1)(i-1)+1}} \exp\{-\lambda_{m_{(2p+1)(i-1)+1}} \times [\theta - (2i-1)\Delta\theta]\} \langle u^+_{m_{(2p+1)(i-1)+1}} | u^+_{n_{(2p+1)i}} \rangle \times A^+(u^-_{n_{(2p+1)i}}, u^+_{n_{(2p+1)(i-1)+1}}) \times F_{i-1}(u^-_{n_{(2p+1)(i-1)+1}}),$$

$$(2i-1)\Delta\theta < \theta \leqslant \left((2i-1)+\frac{1}{2p+1}\right)\Delta\theta, \tag{15d}$$

$$S_-(\theta|\xi_0) = C^-_{m_{(2p+1)(i-1)+(k+1)}} \exp\{-\lambda_{m_{(2p+1)(i-1)+(k+1)}} \times [\theta - (2i-1)\Delta\theta]\} \times \prod_{j=1}^{k} \{\langle u^+_{m_{(2p+1)(i-1)+(j+1)}} | u^-_{m_{(2p+1)(i-1)+j}} \rangle\} \times \exp\left[\frac{\Delta\theta}{2p+1}\left(k\lambda_{m_{(2p+1)(i-1)+(k+1)}} - \sum_{j=0}^{k-1} \lambda_{m_{(2p+1)(i-1)+(j+1)}}\right)\right] \times \langle u^+_{m_{(2p+1)(i-1)+1}} | u^+_{n_{(2p+1)i}} \rangle \times A^+(u^-_{n_{(2p+1)i}}, u^+_{n_{(2p+1)(i-1)+1}}) \times F_{i-1}(u^-_{n_{(2p+1)(i-1)+1}}),$$

$$\left((2i-1)+\frac{k}{2p+1}\right)\Delta\theta < \theta \leqslant \left((2i-1)+\frac{(k+1)}{2p+1}\right)\Delta\theta, \quad k = 1,2,\ldots,(2p-1), \tag{15e}$$

$$S_-(\theta|\xi_0) = C^-_{m_{(2p+1)i}} \exp[-\lambda_{m_{(2p+1)i}}(\theta - 2i\Delta\theta)] \times A^-(u^+_{m_{(2p+1)i}}, u^-_{m_{(2p+1)(i-1)+1}}) \times \langle u^+_{m_{(2p+1)(i-1)+1}} | u^+_{n_{(2p+1)i}} \rangle \times A^+(u^-_{n_{(2p+1)i}}, u^+_{n_{(2p+1)(i-1)+1}}) \times F_{i-1}(u^-_{n_{(2p+1)(i-1)+1}}),$$

$$\left((2i-1)+\frac{2p}{2p+1}\right)\Delta\theta < \theta \leqslant 2i\,\Delta\theta, \tag{15f}$$

where

$$C^+_n = \int_0^\Lambda d\xi\, u^+_n(\xi), \tag{16a}$$

$$C^-_m = \int_0^\Lambda d\xi\, u^-_m(\xi), \tag{16b}$$

$$A^+(u^-_{n_{(2p+1)i}}, u^+_{n_{(2p+1)(i-1)+1}}) = \exp\left[-\left(\frac{\Delta\theta}{2p+1}\right)\lambda_{n_{(2p+1)(i-1)+1}}\right] \times \prod_{j=1}^{2p} \left\{\langle u^-_{n_{(2p+1)(i-1)+(j+1)}} | u^+_{n_{(2p+1)(i-1)+j}} \rangle \times \exp\left[-\left(\frac{\Delta\theta}{2p+1}\right)\lambda_{n_{(2p+1)(i-1)+(j+1)}}\right]\right\}, \tag{16c}$$

$$A^{-}(u^{+}_{m_{(2p+1)i}},u^{-}_{m_{(2p+1)(i-1)+1}}) = \exp\left[-\left(\frac{\Delta\theta}{2p+1}\right)\lambda_{m_{(2p+1)(i-1)+1}}\right] \times\prod_{j=1}^{2p}\left\{\langle u^{+}_{m_{(2p+1)(i-1)+(j+1)}}|u^{-}_{m_{(2p+1)(i-1)+j}}\rangle \times\exp\left[-\left(\frac{\Delta\theta}{2p+1}\right)\lambda_{m_{(2p+1)(i-1)+(j+1)}}\right]\right\}, \tag{16d}$$

and the functions F_i are generated through the recursion relation:

$$F_i(u^{-}_{n_{(2p+1)i+1}}) = \langle u^{-}_{n_{(2p+1)i+1}}|u^{-}_{m_{(2p+1)i}}\rangle \times A^{-}(u^{+}_{m_{(2p+1)i}},u^{-}_{m_{(2p+1)(i-1)+1}}) \times\langle u^{+}_{m_{(2p+1)(i-1)+1}}|u^{+}_{n_{(2p+1)i}}\rangle \times A^{+}(u^{-}_{n_{(2p+1)i}},u^{+}_{n_{(2p+1)(i-1)+1}}) \times F_{i-1}(u^{-}_{n_{(2p+1)(i-1)+1}}), \tag{17}$$

with $F_0(u^{-}_{n_1})=u^{-}_{n_1}(\xi_0)$. The angular brackets in the above equations imply a dot product of the corresponding functions, for, e.g.,

$$\langle u^{+}|u^{-}\rangle = \int_0^{\Lambda} d\xi\, u^{+}(\xi)u^{-}(\xi). \tag{18}$$

The cycle variable i runs over positive integers; i.e., $i=1,2,3,\ldots$. The positive and negative symbols of the survival probabilities indicate their value over the positive and negative part of the cycles, respectively. In all these expressions, viz., Eqs. (15)–(17), for any subscript, either n or m or both, wherever they appear more than once, the summation over them is implied. The effect of history is explicit in the expressions for survival probabilities. Once the survival probability $S(\theta|\xi_0)$ is obtained from these formulas, the FPTDF, MFPT, and the corresponding variance are obtained by employing Eqs. (13) and (14). Evaluation of MFPT and other relevant quantities requires the sum of infinite series, which must be truncated in order to obtain a final result. Convergence of MFPT is ensured by gradually increasing the number of terms (i.e., number of eigenvalues) for the calculation. The process is truncated when MFPT does not change up to two decimal points of accuracy with the change of the number of terms.

III. RESULTS AND DISCUSSIONS

The survival probability, mean first passage time (MFPT), corresponding variances, and first-passage time density functions (FPTDF) are calculated using the derived formulas for this process. The results are summarized below.

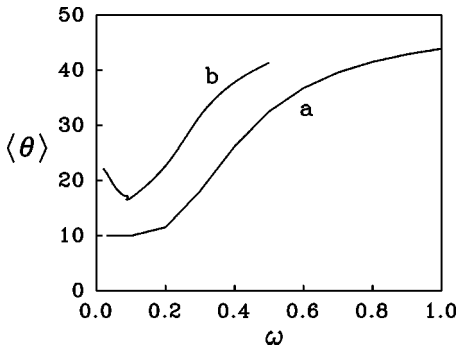

FIG. 2. MFPT $\langle\theta\rangle$ as a function of ω; (a) for $p=0$; the usual telegraph signal (b) for $p=1$; the two-step periodic signal ($\Lambda=20,\xi_0=\Lambda/2$).

A. General features of CSR

The MFPT is calculated for a single-step telegraph signal ($p=0$) with $\xi_0=\Lambda/2$. Most of the calculations are done with this specific value of ξ_0. The variation of the results with the variation of ξ_0 is also demonstrated (see the text below). No nonmonotonous behavior is observed in MFPT as we vary the frequency ω. This is in complete agreement with Porra's observation [9]. The calculation is done for the length $\Lambda=20$ and the result is shown in the curve *a* of Fig. 2. However, when we take $p=1$, i.e., when the sinusoidal signal is approximated by a two-step periodic signal, the calculation of MFPT for the same length shows clearly the nonmonotonic behavior. This is shown in curve *b* of the same figure. This result clearly demonstrates that mere flipping of the bias (signal) direction periodically would not produce the coherent motion. As the rate of flipping increases, it merely prevents the particle from reaching the boundaries and therefore MFPT increases monotonically. It may be noted that when the flipping rate is very high, the effect of the signal is almost nonexistent and the transport is effectively diffusive in nature. This is of course true in any type of periodic signal. Therefore, for any type of approximation of the sinusoidal signal or for any value of p, this feature would show up. In particular, for $p=1$, we observe from curve *b* of Fig. 2 that MFPT asymptotically reaches the diffusive limit $\Lambda^2/8$ ($=50$ in this case). The usual telegraph signal offers a constant bias of maximum magnitude for the larger time than for a two-step approximation. Hence the particle always has a larger probability of reaching the boundary in short time for the $p=0$ case than for the $p>0$ case. Hence MFPT for the $p=0$ and for any ω is always less than for $p>0$ case. This is observed in Fig. 2.

The application of any bias always reduces the MFPT below that for the nonbiased diffusion. In CSR we always have a competition between diffusion and the oscillatory effect of the bias. For very large frequency, as the bias effect becomes ineffective, MFPT would essentially be guided by the diffusive process. For zero frequency of the multistep periodic signal, the MFPT can be analytically evaluated. When it starts from the midpoint of the medium, it is expressed as $\langle\theta(\omega=0,\xi_0=\Lambda/2)\rangle=0.5(\Lambda/s_1)\tanh(s_1\Lambda/4)$. When the frequency is very small, the process is predominantly diffusion with a constant value $s_1=0.5\sin(\pi/2p+1)$ effective for $0<\theta\leqslant\pi/\omega(2p+1)$. However, as the frequency increases slowly, the probability of having an in-

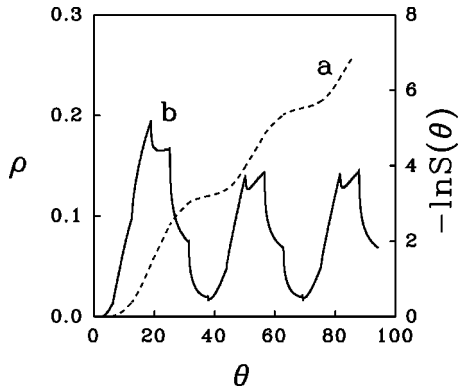

FIG. 3. (a) $-\ln S(\theta)$ as a function of θ (dashed curve). (b) The decay rate, ρ, as a function of θ (solid curve) ($\Lambda=20, \xi_0=\Lambda/2, p=2, \omega=0.1$).

creased bias value s_2 ($=1$ for $p=1$) before it reaches the boundary increases. This bias force reduces the survival probability and also MFPT. Hence one would expect a minimum MFPT. On the other hand, for the usual telegraph signal (the $p=0$ case), for very low frequency, from the very beginning bias force affects the particle with its maximum strength. When the frequency is very low, this constant bias diffusion continues for a longer time and there is no changeover of the magnitude of the bias as in the case of $p=1$. After having a flip, the particle again suffers a constant bias diffusion in the direction opposite to the previous one. As frequency increases slowly, this picture remains unchanged until a stage is reached for which the flipping effect becomes dominant during the particle's survivability inside the medium and MFPT increases. This is observed in Fig. 2.

Next we continue all our calculations with $p=2$ or with the three-step telegraph signal. Calculation reveals that the value of MFPT does not change much from that with $p=1$. On the other hand, the $p=2$ signal approximates better than the $p=1$ signal. We restrict our calculation to the $p=2$ approximation of the periodic signal.

Typical survival probability and the corresponding decay rate defined as $\rho(\theta)=-[dS(\theta)/d\theta]/S(\theta)$ are plotted as a function of θ for $\Lambda=20$ and $\omega=0.1$ in Fig. 3. The plot shows that the survival probability [plot (a)] goes through the plateau where the change of survival probability is comparatively less. The decay rate $\rho(\theta)$ [plot (b)] correspondingly shows a minimum at these points. This is a characteristic feature for CSR. This feature is in agreement with the numerical simulation of the process as a random walk on a lattice [7].

Next we calculate the MFPT $\langle\theta\rangle$ and the variance σ^2 as a function of frequency ω for different lengths ($\Lambda=10,20,30,40,50$). These are presented in Fig. 4 and Fig. 5, respectively. Both the cumulants go through a minimum as the frequency rises from a very low value for each length Λ. This feature is also in agreement with the lattice simulation work [7]. It is observed that the minimum for both moments occurs at the same frequency for each length. The value of MFPT $\langle\theta\rangle$ increases with length at all frequencies. This is understandable because as the length increases, on average the particle will spend more time in the medium before reaching the boundaries. It is also observed that the frequency at which the minimum occurs shifts toward low frequency as the length increases. It implies that the maximum cooperation between the deterministic signal and random noise occurs at lower frequencies as the length increases. For low resonant frequency, the particle is affected by the bias in a particular direction for a longer period of time before it suffers a change in the direction of bias, thus there is a higher probability of covering a large distance toward the boundary, and at this resonant frequency the probability of reaching the boundary in a short time is maximum because if one increases the frequency more than the resonant frequency at that length, the flipping rate dominates and the average time taken by the particle is greater.

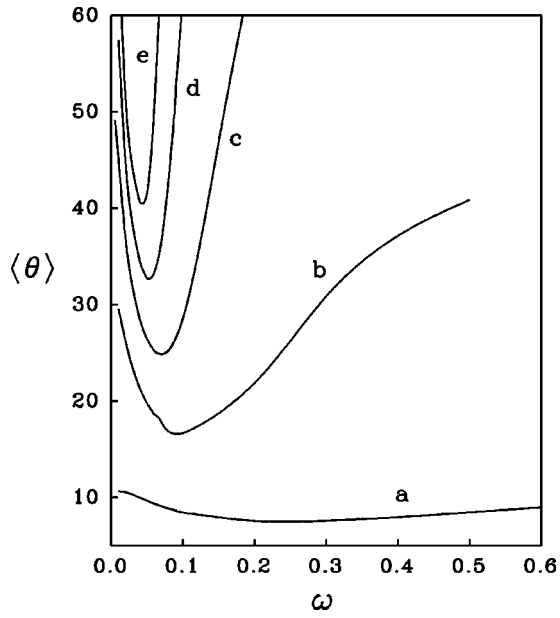

FIG. 4. MFPT $\langle\theta(\omega)\rangle$ as a function of frequency ω; (a) $\Lambda=10$, (b) $\Lambda=20$, (c) $\Lambda=30$, (d) $\Lambda=40$, (e) $\Lambda=50$ ($p=2, \xi_0=\Lambda/2$).

Figure 5 demonstrates the lowering of the dispersion at resonant frequencies, confirming that the cooperation is maximum at these frequencies. Dispersion is greater for

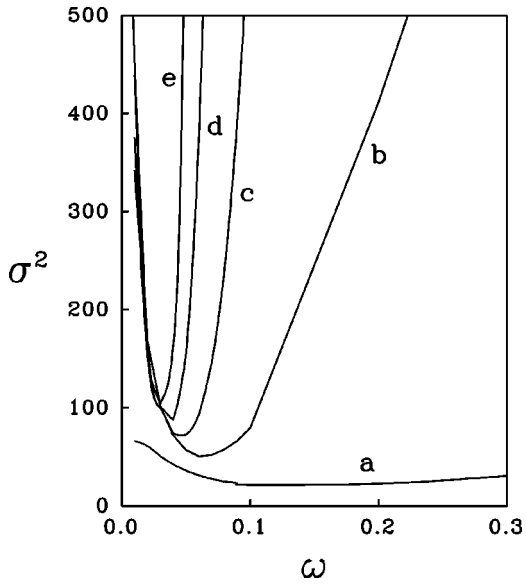

FIG. 5. The variance σ^2 as a function of ω; (a) $\Lambda=10$, (b) $\Lambda=20$, (c) $\Lambda=30$, (d) $\Lambda=40$, (e) $\Lambda=50$ ($p=2, \xi_0=\Lambda/2$).

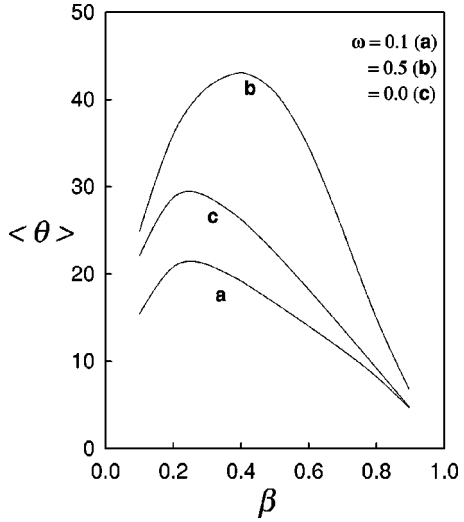

FIG. 6. MFPT $\langle\theta\rangle$ as a function of β for length $\Lambda=20$; (a) for resonant frequency $\omega^*=0.1$; (b) for off-resonant frequency $\omega=0.5$; (c) for off-resonant frequency $\omega=0.0$ ($p=2$).

higher lengths, and as seen from the figure the dispersion merges to a specific value at very low frequency at various lengths.

All the previous calculations are done when the particle starts initially from the midpoint of the medium, i.e., ξ_0 in Eqs. (15) is taken as $\Lambda/2$. At the length $\Lambda=20$, the resonant frequency is found to be 0.1. The calculations are done with one at resonant frequency and the other two at the off-resonant frequencies ($\omega=0.5$ and $\omega=0.0$) when the particle starts from $\xi_0=\beta\Lambda$, where β lies between 0 and 1. For zero frequency, the MFPT can be analytically obtained. Its expression reads $\langle\theta(\omega=0,\beta\Lambda)\rangle=(\Lambda/s_1)\{-\beta+(1-\exp[-s_1\beta\Lambda])/(1-\exp[-s_1\Lambda])\}$. The curves are shown in Fig. 6. It is evident that the value of $\langle\theta\rangle$ is lower for resonant frequency (curve *a*) than for its value for off-resonant frequencies (curves *b* and *c*). As frequency increases, the maximum value of $\langle\theta\rangle$ occurs at lower values of β or when the particle starts from the left of the interval. It is known that for pure diffusion, the location of the maximum $\langle\theta\rangle$ would occur for $\beta=0.5$. Our signal starts with the positive half-cycle and therefore the survival time of the particle would be greater if the particle started from the left of the interval. Of course there would be some limit, because if it started too close to the left end, then diffusion towards the left boundary would dominate and the average time would be less. On the other hand, if it started from the right half of the medium, the initial surge of the signal would help the particle to reach the boundary more quickly. Hence the average time of duration would decrease. This fact is also in agreement with lattice simulation work [7], although most of the simulations in [7] were obtained for a uniformly distributed initial condition.

We next calculate the FPTDF $g(\theta)$ for various frequencies for $\Lambda=20$ and plot the curves in Fig. 7. The resonant frequency for this length is found to be 0.1. Before the resonant frequency is reached, $g(\theta)$ has got two distinct peaks [Fig. 7(a)] and at resonance two peaks merge to a single large peak. After the resonance, many smaller peaks in $g(\theta)$ gradually emerge as frequency increases more than the resonant frequency [Fig. 7(b)]. This is a general characteristic of CSR. The height h and the position θ_p of the first peak as a

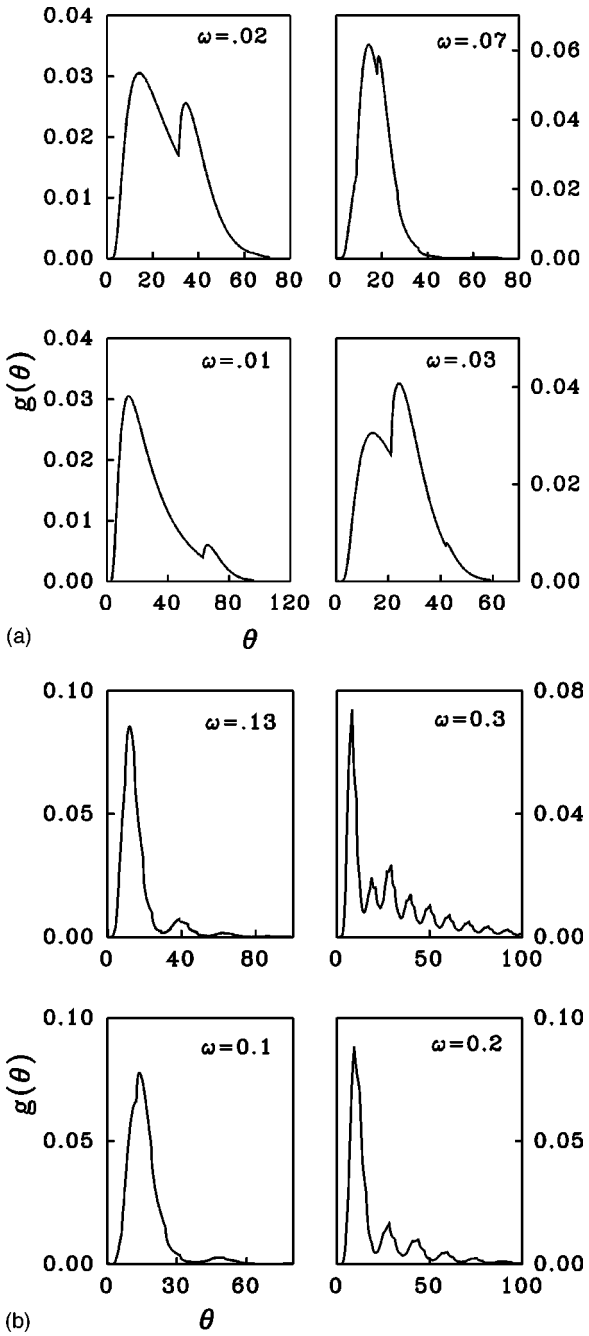

FIG. 7. (a) FPTDF $g(\theta)$ as a function of θ for $\Lambda=20$ before resonance for frequencies $\omega=0.01,0.02,0.03,0.07$; (b) FPTDF $g(\theta)$ as a function of θ for $\Lambda=20$ on and after resonance for frequencies $\omega=0.1$ (resonant), $\omega=0.13,0.2,0.3$, respectively ($p=2,\xi_0=\Lambda/2$).

function of ω are plotted in curve *a* of Fig. 8. The figure shows that the height of the first peak goes through a maximum as we increase the frequency while the position of that peak remains practically constant. The height reaches the maximum near the resonant frequency, demonstrating that the probability of reaching the boundary in a short time is maximum near the resonant frequency. It is a kind of reflection of having $\langle\theta\rangle$ minimum at that frequency. Therefore, it is a general characteristic of CSR. The height and position of the second peak before the resonance are drawn as curve *b* in Fig. 8. At resonance, the two peaks merge and we have only one peak. Just after the resonance, another peak starts developing and height increases as frequency increases further.

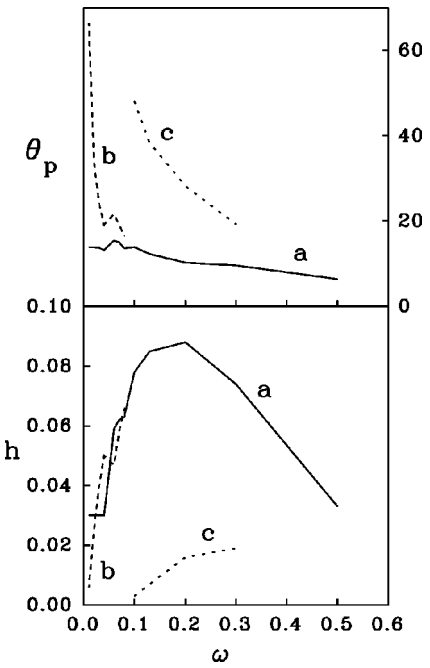

FIG. 8. Height h and the position of the peak θ_p as a function of ω; (a) for the first peak (solid curve); (b) for the second peak before resonance (dashed curve); (c) for the second peak after resonance (dotted curve).

The position and height of the second peak after resonance are plotted in curve *c* of the same figure. The merging and the reappearance of the second peak are also observed as a brake or discontinuity of the dashed line in this figure.

B. Universal features at resonance

In this subsection we concentrate on the behavior of the system at the resonance point. We have already discussed some general characteristics of CSR in the preceding subsection. We find that for each length, Λ, a corresponding frequency ω^* exists for which $\langle\theta\rangle$ and σ^2 become minimum, implying that the maximum cooperation between the deterministic periodic signal and the random noise of the environment is taking place in helping the particle to reach the boundaries. One therefore would naturally inquire about the relation of ω^* with Λ. The curve of ω^* as a function of Λ is plotted in Fig. 9. In the range of Λ that we studied, this curve is very well fitted with the formula

$$\omega^* = 2/\Lambda. \tag{19}$$

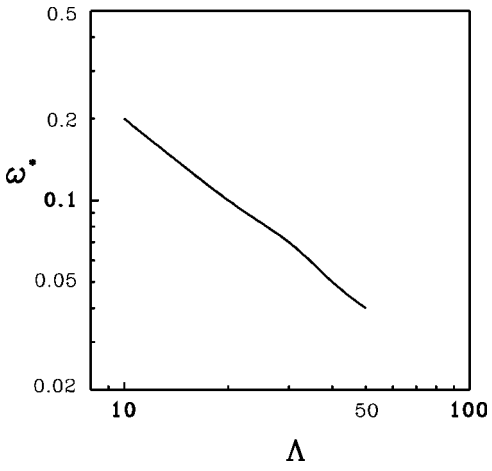

FIG. 9. Resonant frequency ω^* as a function of length Λ.

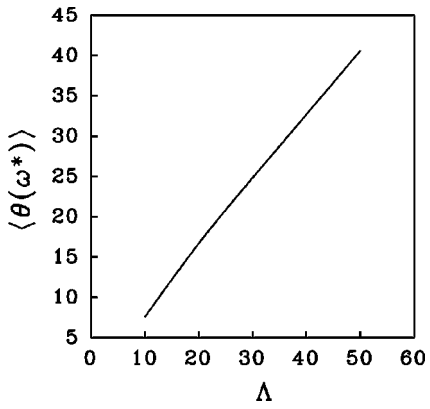

FIG. 10. MFPT at the resonant frequency $\langle\theta(\omega^*)\rangle$ as a function of length Λ.

The values of MFPT at resonance $\langle\theta(\omega^*)\rangle$ are plotted against the length Λ in Fig. 10 and within the range of Λ we consider the relation between them is fitted to

$$\langle\theta(\omega^*)\rangle = 0.82\Lambda - 0.14. \tag{20}$$

Of course, there will be deviation from this linear behavior as Λ decreases further because $\langle\theta\rangle$ cannot become negative and for $\Lambda=0$ (corresponding to $L=0$), $\langle\theta\rangle$ should be zero.

Similarly the variance $\sigma^2(\omega^*)$ is plotted as a function of Λ in Fig. 11, and within the range of Λ that we consider, this curve is fitted to

$$\Lambda = a[\sigma^2(\omega^*)]^2 + b, \tag{21}$$

with $a=0.004$ and $b=9.29\pm0.82$.

We have already seen that at the resonance frequency we have one very dominant peak of FPTDF, $g(\theta)$ [Fig. 7(b)]. Since it is a general feature, for each length Λ we should get such behavior. We further observe that ω^* varies inversely with Λ [Eq. (19)]. With this fact in mind when we plot $g(\theta)/\omega^*$ as a function of $[\omega^*(\Lambda)\theta]$, we find that curves for all lengths superpose over each other (Fig. 12) and the pattern of $g(\theta)/\omega^*$ for different Λ or ω^* is very similar, i.e., at

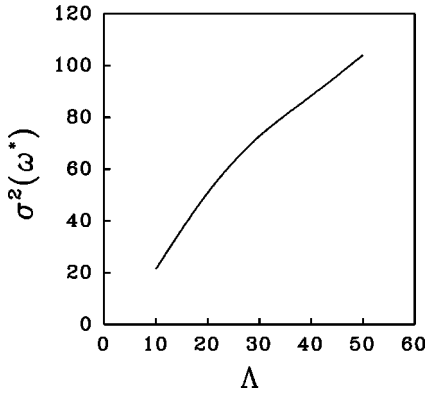

FIG. 11. The variance at the resonant frequency $\sigma^2(\omega^*)$ as a function of the length Λ.

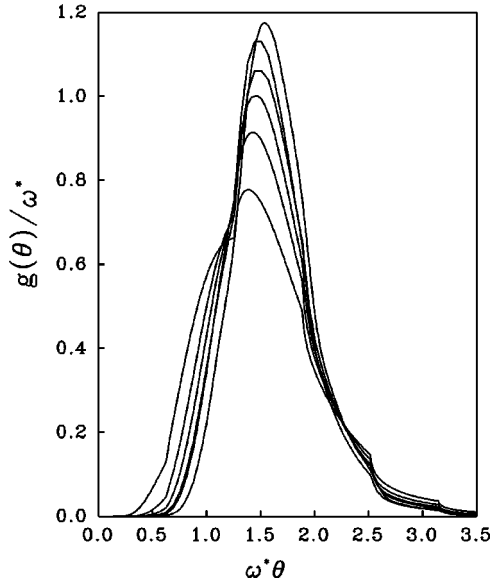

FIG. 12. The dominant peaks of $g(\theta)/\omega^*$ at resonant frequencies for different lengths ($\Lambda=20,28.57,35,40,44.44,50$) as a function of $\omega^*\theta$. The lowermost curve is for $\Lambda=20$, and as length increases gradually upper curves are generated ($p=2,\xi_0=\Lambda/2$).

particular values of $[\omega^*\theta]$ all curves show their maxima, minima, and change in the behavioral patterns of the curves occur exactly at the same places of $[\omega^*\theta]$. Similar characteristics are also observed in the curves of decay rate ρ for different frequencies. For illustration, we plot ρ as a function of $[\omega^*\theta]$ for three different lengths ($\Lambda=20$, curve *a*; $\Lambda=28.57$, curve *b*; $\Lambda=15.38$, curve *c*), and present the results in Fig. 13. Therefore, it shows that this feature is universal and $[\omega^*\theta]$ or the cycle number is the correct variable to describe the resonance behavior. We may further note that such scaling of FPTDF would not be possible for any frequency other than the resonant frequencies, because any frequency which is not the resonant frequency for one length may turn out to be the resonant frequency for some other length, and the features of FPTDF are different for resonant and off-resonant frequencies, as has been observed from Figs. 7(a) and 7(b). The major dominant peaks of FPTDF $g(\theta)/\omega^*$ for different lengths ($\Lambda=20,28.57,35,40,44.44,50$) are drawn as a function of $[\omega^*\theta]$ in Fig. 12. The lowermost curve is for $\Lambda=20$, and as the length increases the upper curves are generated. The peaks for all the curves occur nearly at a quarter of a cycle.

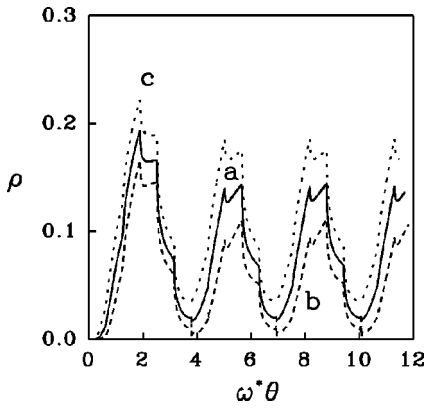

FIG. 13. The decay rate ρ for different resonant frequencies as a function of $\omega^*\theta$: (a) $\Lambda=20,\omega^*=0.1$ (solid curve); (b) $\Lambda=28.57,\omega^*=0.07$ (dashed curve); (c) $\Lambda=15.38,\omega^*=0.13$ (dotted curve) ($p=2,\xi_0=\Lambda/2$).

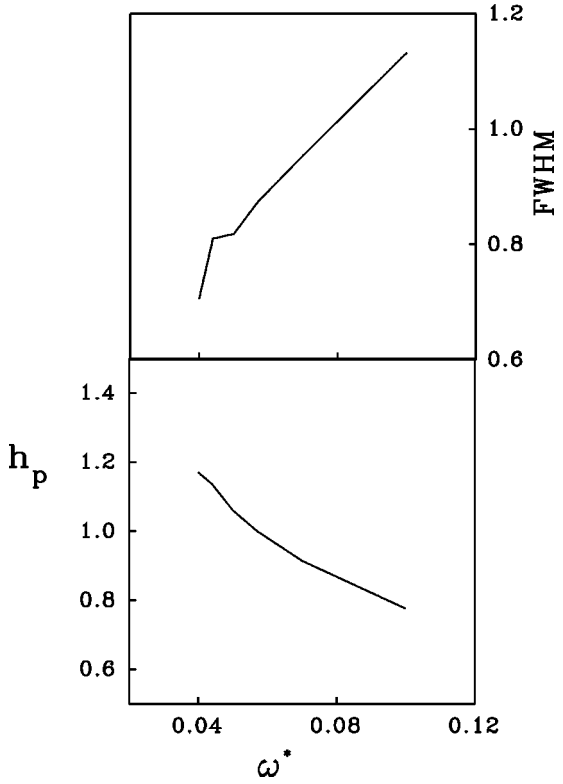

FIG. 14. The height h_p and full width at half maximum (FWHM) of the peaks in Fig. 12 are plotted as a function of their corresponding resonant frequencies.

The peak height h_p and full width at half maximum (FWHM) for each curve are plotted as a function of resonant frequency. The plot is given in Fig. 14. The plot shows that except for very low frequency, they behave linearly with the resonant frequency.

C. Behavior around the resonant point

We have already seen that the cooperation between the deterministic signal and the random noise is maximum at the resonance point where MFPT $\langle\theta\rangle$ variance σ^2 takes minimum values and the corresponding FPTDF $g(\theta)$ shows a major dominant peak. What would happen when we change the frequency slightly above and below the resonant frequency? To investigate the matter, we choose a particular length of the medium, $\Lambda=20$. The resonance frequency for such a length $\omega^*=0.1$. For this particular length, we take two off-resonant frequencies $\omega=0.07$ and $\omega=0.13$. The curves for survival probabilities as a function of time θ are plotted in Fig. 15, where the curves *a,b,c* are for frequencies $\omega=0.1,0.07,0.13$, respectively. The calculation of the survival probability is terminated when it takes the value 1×10^{-3}, which corresponds to zero in our calculation. The curves clearly show that as frequency increases, the survivability of the particle is prolonged. This is quite understandable because more oscillations prevent the particle from

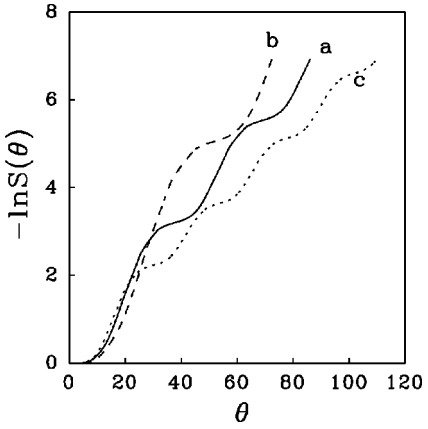

FIG. 15. $-\ln S(\theta)$ as a function of time θ: (a) $\Lambda=20,\omega^*=0.1$ (solid curve); (b) $\Lambda=20,\omega^*=0.07$ (dashed curve); (c) $\Lambda=20,\omega^*=0.13$ (dotted curve) ($p=2,\xi_0=\Lambda/2$).

reaching the boundary, i.e., for higher frequency we expect $\langle\theta\rangle$ more. The oscillatory effect is more pronounced when time is large. For large time, we always expect the value of $S(\theta)$ more for higher frequency. This is clearly observed in Fig. 15. But for frequencies lower than the resonant frequency, MFPT $\langle\theta\rangle$ is again more. As MFPT is the integral of the survival probability over time, we expect a change in the behavior of $S(\theta)$ for the lower time regime. This is shown explicitly in Fig. 16. In this figure we find that the survival probability is greater for low frequency, $\omega=0.07$ (curve *b*), than for resonant frequency, $\omega^*=0.1$ (curve *a*), and off-resonant frequency $\omega=0.13$ (curve *c*). Especially for curve *b*, the value of *S* is much greater than that for curve *a*, so that the area under curve *b* is more than that for curve *a*. We see that near about $\theta=28$, the solid curve crosses the dashed curve. There is only one point of crossing throughout the entire time. We have already argued that after this crossing point, the oscillatory effect of this bias dominates. It is then clear for the low time regime that the diffusion process competes over the oscillatory effect. Again, for very low θ the chance of having an increased value of the bias in the same direction is greater for high frequency than for low frequency. Therefore, for low frequency the survivability is greater than for high frequency. The curves in Fig. 16 also demonstrate that.

We have already demonstrated how $\langle\theta(\omega^*)\rangle$ varies with Λ in Fig. 10. The behavior is linear with respect to the length

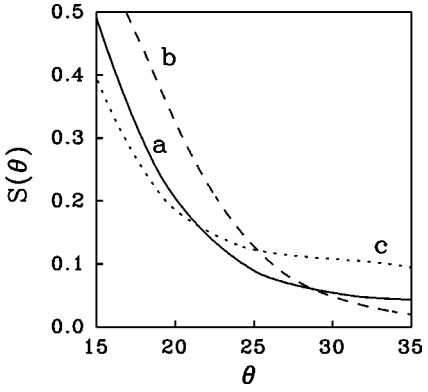

FIG. 16. $S(\theta)$ as a function of θ for the same curves as in Fig. 15.

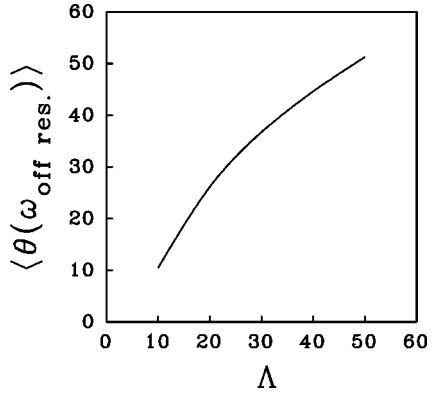

FIG. 17. MFPT at off-resonant frequency $\langle\theta(\omega_{\text{off-res.}})\rangle$ as a function of Λ ($p=2,\xi_0=\Lambda/2$).

of the medium. It is of interest whether the behavior is changed for off-resonant frequency. For that we choose a frequency which is not the resonant frequency for the lengths Λ that we consider in our calculation. The MFPT $\langle\theta(\omega)\rangle$ for that off-resonant frequency is calculated for different lengths and is plotted as a function of Λ in Fig. 17. For the range of length we consider that the curve is fitted to

$$\Lambda=a'\langle\theta(\omega_{\text{off-res}})\rangle^2+b' \tag{22}$$

with $a'=0.016$ and $b'=8.68\pm0.33$. We may note that this particular off-resonant frequency would be a resonant frequency for some length, Λ_0, governed by Eq. (19). In our case this off-resonant frequency corresponds to length $\Lambda_0>50$. The curve shows that when $\Lambda\ll\Lambda_0$, the rate of change of MFPT with respect to Λ is greater, and when Λ approaches Λ_0 or when this frequency tends to be the resonant frequency, the rate is curbed. This could be a signature of approaching a coherent motion from the noncooperative behavior.

IV. CONCLUDING REMARKS

We consider a diffusive transport process perturbed by a periodic signal in a continuous one-dimensional medium having two absorbing boundaries. No perturbation approximation of the signal amplitude is assumed in this formulation. We showed explicitly that the cooperative behavior between the deterministic periodic signal and random noise leading to coherent motion occurs when the time-dependent sinusoidal signal is approximated by a multistep periodic signal and not with a single-step telegraph signal.

Although we study the process with a three-step periodic signal, the formulation is quite general and applicable for any approximation with an arbitrary number of steps. This formulation can also be applied to any arbitrary continuous periodic signal.

It is observed that for large times, oscillation of the signal plays a dominant role in the transport, while in the low time regime, frequency-dependent bias force (i.e., the chance of having an increased value of the bias in the same direction is more for high frequency than for low frequency) has the key factor. For very high frequency, the bias effect is practically absent and the motion is purely diffusive in nature. At the resonance, the maximum cooperation between the noise and

the periodic signal takes place.

An important characteristic that we observe is that at the resonance the FPTDF for various lengths have similar behavior to a function of cycle number. There is only one dominant peak and the peak position occurs very close to a quarter of a cycle. From Fig. 12 we observe a slight deviation of the peak positions, but we believe that if the sinusoidal signal is approximated by more than a three-step periodic signal, the positions of all the peaks will be the same.

There is also a slight discrepancy in the position of the minimum of σ^2 in comparison to the minima of $\langle \theta \rangle$ (Figs. 4 and 5). This may be due to the fact that all calculations are terminated when the survival probability takes a value 1×10^{-3}. We observe that if we cut off the calculations for lower values of survival probability, it does not affect MFPT but the variances are slightly affected. Also if one approximates the sinusoidal signal better than a three-step periodic signal, one could obtain the positions of the minima of variances at exactly the same places as those with MFPT.

It is interesting to observe that the decay rate at the resonance (Fig. 13) after $\omega^* \theta = 5\pi/4$ is clearly a periodic function of time.

[1] D. C. Schwartz and C. R. Cantor, Cell **37**, 67 (1984).
[2] G. F. Carle, M. Frank, and M. V. Olson, Science **232**, 65 (1986).
[3] I. J. Lin and L. Benguigi, Sep. Sci. Technol. **20**, 359 (1985).
[4] G. H. Weiss, Adv. Chem. Phys. **13**, 1 (1967).
[5] C. W. Gardiner, *A Handbook of Stochastic Methods*, 2nd ed. (Springer-Verlag, New York, 1985).
[6] N. G. van Kampen, *Stochastic Processes in Physics and Chemistry* (North-Holland, Amsterdam, 1991).
[7] J. E. Fletcher, S. Havlin, and G. H. Weiss, J. Stat. Phys. **51**, 215 (1988).
[8] J. Masoliver, A. Robinson, and G. H. Weiss, Phys. Rev. E **51**, 4021 (1995).
[9] J. M. Porra, Phys. Rev. E **55**, 6533 (1997).